TABLE 1 Design Data

Design Data			
a (mm)	b (mm)	x' (mm)	y' (mm)
40.945	41.744	14.409	15.653

using Boulder Microwave Technologies's Ensemble 5.1. The simulated bandwidth for VSWR = 2.0 is 52 MHz (2.3%), and the bandwidth for an axial ratio less than 3 dB is 13 MHz (0.51%). The return loss at the resonance frequency is 27.6 dB, and the axial ratio is 0.63 dB.

The measured center frequency is 2.212 GHz, which shows a 1.7% error for the 2.25 GHz design frequency. The measured bandwidth is 60 MHz, and the return loss is -28.8 dB at the 2.212 GHz center frequency. Figure 3 compares the designed axial ratio with the simulated one using Ensemble. The axial ratio simulated by Ensemble is 1.25 dB at 2.241 GHz, which shows a 0.04% difference for the design data. The bandwidth for an axial ratio less than 3 dB is 14 MHz.

V. CONCLUSION

In this paper, we have presented a new design method for a coaxially fed circularly polarized rectangular microstrip antenna using a GA. The usefulness of a GA for the complicated object function was illustrated by designing the circularly polarized microstrip antenna. The size and the feeding point were optimized for the given substrate properties and the operating frequency. The computed return loss was 27.6 dB, the bandwidth was 52 MHz (2.3%), and the operating frequency showed a 1.7% error for the measured data. The axial ratio bandwidth was 13 MHz (0.51%), and showed a 0.04% difference for the simulated data using Ensemble.

REFERENCES

1. J. Bahl and P. Bhartia, Microstrip antennas, Artech House, Dedham, MA, 1980.
2. J.R. James and P.S. Hall, Handbook of microstrip antennas, Peter Peregrinus Ltd., London, England, 1989.
3. P.C. Sharma and K.C. Gupta, Analysis and optimized design of single feed circularly polarized microstrip antennas, IEEE Trans Antennas Propagat AP-31 (1983), 949–955.
4. D. Thouriude, M. Himdi, and J.P. Daniel, Synthesis of microstrip or coaxially fed rectangular patch antennas, IEICE Trans Commun E79 B (1986), 871–874.
5. D. Thouriude, M. Himdi, and J.P. Daniel, CAD-oriented cavity model for rectangular patches, Electron Lett 26 (1990), 842–844.
6. F. Lumini, L. Cividanes, and J.C. da S. Lacava, Computer aided design algorithm for singly fed circularly polarized rectangular microstrip patch antennas, Int J RF & Microwave Computer-Aided Eng 9 (1999), 32–41.
7. E.D. Goldberg, Genetic algorithms in search, optimization and machine learning, Addison-Wesley, Reading, MA, 1989.
8. L. Chambers, Practical handbook of genetic algorithms, New frontiers, Vol. 2, CRC Press, Boca Raton, FL, 1995.
9. Y.T. Lo, D. Solomon, and W.F. Richards, Theory and experiment on microstrip antenna, IEEE Trans Antennas Propagat AP-27 (1979), 137–145.
10. W.F. Richard, Y.T. Lo, and D.D. Harrison, An improved theory for microstrip antennas and applications, IEEE Trans Antennas Propagat AP-29 (1981), 38–46.
11. D.M. Pozar, Improved computational efficiency for the moment method solution of printed dipoles and patches, Electromagnetics 3 (1983), 299–309.
12. K.F. Lee and W. Chen, Advances in microstrip and printed antennas, Wiley, New York, 1997.
13. D.R. Jackson and N.G. Alexapoulos, Simple approximate formulas for input resistance, bandwidth, and efficiency of a resonant rectangular patch, IEEE Trans Antennas Propagat 39 (1991), 407–410.
14. D.M. Pozar, Rigorous closed-form expressions for the surface-wave loss of printed antennas, Electron Lett 26 (1990), 954–956.
15. C.A. Balanis, Antenna theory: Analysis and design, Wiley, New York, 1982.

THERMAL IMPEDANCE MODEL OF ELECTROSTATIC DISCHARGE EFFECTS ON MICROBOLOMETERS

F. J. González,[1] C. Fumeaux,[1] J. Alda,[2] and G. D. Boreman[1]
[1] School of Optics / CREOL
University of Central Florida
Orlando, Florida 32816-2700
[2] Department of Optics
School of Optics
University Complutense of Madrid
28037 Madrid, Spain

Received 6 March 2000

ABSTRACT: *The small thermal mass of microbolometers, used in antenna-coupled infrared detectors, makes them especially vulnerable to electrical stress caused by electrostatic discharge (ESD). In this paper, an empirical thermal model, which is independent of the device geometry, is used to characterize the behavior of microbolometers under ESD conditions. The parameters of this thermal model are fitted to measurements made on the microbolometers, and a power-to-failure versus time-to-failure curve is obtained.* © 2000 John Wiley & Sons, Inc. Microwave Opt Technol Lett 26: 291–293, 2000.

Key words: *microbolometer; antenna-coupled infrared detector; ESD; thermal model*

I. INTRODUCTION

Bolometer operation is based on the change in the electrical resistance of a material as a function of temperature. In the case of microbolometers, where the dimensions of the sensor are much smaller than the wavelength, an antenna is needed to couple power into the temperature-sensitive element [1, 2]. The coupling of power to sensors of small thermal mass yields large changes in temperature, and consequently high responsivity. The fact that the thermal mass of the microbolometer is small also makes the detector fast. This is a valuable characteristic for a wide range of applications, but it makes the detector vulnerable to other factors, such as joule heating caused by the bias voltage or other types of electrical stress. Electrostatic discharge (ESD) is a transient current arising from induced static charge. The voltages generated by ESD can be as high as 20 kV, depending on the charge accumulated and the capacitance of the element, which is the source of the discharge. In a typical situation, a charge of 0.6 μC can be induced easily in a human body of a capacitance of 150 pF, which yields an electrostatic potential of 4 kV [3]. The discharge current exists in a very short period of time, typically on the order of hundreds of nanoseconds, with currents ranging from 1 to 10 A [3]. Permanent damage generally occurs when the temperature of the bolometer material exceeds its melting point.

In order to implement effective protection against ESD events, the behavior of the device in question under ESD conditions must be known. The most accurate way of predicting the effects of an ESD event in any device is to analyze the heat dissipated in the device during a high-current stress event [4]. An analytical approach to this is to solve the heat conduction equation for the particular device geometry under consideration:

$$\frac{\partial T}{\partial t} - D \cdot \nabla^2(T) = \frac{q(t)}{\rho \cdot C_p} \tag{1}$$

where ρ is the density of the material, C_p is the specific heat, D is the thermal diffusivity, and $q(t)$ is the rate of heating per unit volume of the heat source. This procedure requires the solution of a partial differential equation subject to boundary conditions from the geometry of the device under consideration. In the general case, the solution of Eq. (1) can be quite involved.

II. METHOD

Here, we present a simpler approach that is independent of the microbolometer's geometry. This approach uses an equivalent thermal circuit consisting of a parallel combination of a thermal resistance and a thermal capacitance [5]. The thermal impedance Z_{th} for our model is given by

$$Z_{th}(s) = \frac{R_{th}}{1 + s \cdot R_{th} \cdot C_{th}} \tag{2}$$

where R_{th} and C_{th} are the thermal resistance and capacitance of the bolometer, and s is the Laplace complex-frequency variable. The rise in temperature (ΔT) in the device under ESD stress is given by

$$\Delta T = T - T_0 = P \cdot Z_{th} \tag{3}$$

where P is the power dissipated, T is the final temperature, and T_0 is the initial temperature. We assume, as a worst case scenario, that all power generated by the ESD event is dissipated in the device. The transmission-line pulsing (TLP) method is used to characterize the ESD event [6], modeling it as a square pulse with a width in the 100–200 ns range. The power is given by

$$P_{ESD} = \frac{V_{ESD}^2}{R_b} \tag{4}$$

where V_{ESD} is the electrostatic potential generated and R_b is the electrical dc resistance of the microbolometer. The Laplace domain expression for the power generated by an ESD event is

$$P(s) = \frac{V_{ESD}^2}{R_b} \cdot \left(\frac{1 - e^{-\tau \cdot s}}{s} \right) \tag{5}$$

where τ is the duration of the ESD pulse. The temperature of the bolometer as a function of time [Eq. (3)], which results from an ESD event, can be found by the inverse transform of the product of the thermal impedance [Eq. (2)] and the power generated [Eq. (4)]:

$$T(t) = L^{-1}\{Z_{th}(s)P(s)\} \tag{6}$$

$$T(t) = \frac{R_{th} \cdot V_{ESD}^2}{R_b} \times \left[1 - e^{\frac{-t}{R_{th} \cdot C_{th}}} + \left(e^{\frac{\tau - t}{R_{th} \cdot C_{th}}} - 1 \right) \cdot u(t - \tau) \right] + T_0 \tag{7}$$

where $u(t - \tau)$ is the unit-step function. Equation (7) shows that the temperature is a function of the measured characteristics of the bolometer R_{th}, C_{th}, and R_b, and of the characteristics of the ESD event V_{ESD} and τ. A typical temperature response resulting from an applied voltage can be seen in Figure 1, where the case of a square pulse with $\tau = 200$ ns and $V_{ESD} = 1$ V is considered.

The responsivity of the bolometer is the output voltage per unit input power (V/W), and is given by

$$\Re = \alpha \cdot |Z_{th}| \cdot V_b \tag{8}$$

where α is the temperature coefficient of resistance of the sensor material and V_b is the dc bias voltage across the device [7]. Plotting the bolometer's response (in volts) per incident power as a function of the modulation frequency yields the responsivity curve. Using Eqs. (2) and (8), values for R_{th} and C_{th} can be obtained, noting that R_{th} determines the dc responsivity, and that the product of R_{th} and C_{th} represents the time constant of the device.

III. RESULTS AND DISCUSSION

The proposed thermal model was fitted to measurements made on antenna-coupled niobium microbolometers with a mean dc resistance of $R_b = 195\ \Omega$. These bolometers are used for the detection of infrared radiation with wavelengths around 10 μm. The sensing element is a niobium patch of dimensions 1.5 μm × 350 nm with 50 nm thickness [8]. The responsivity measurements were made using a focused CO_2-laser beam with a wavelength of 10.6 μm and an acousto-optic modulator [9]. Figure 2 compares the thermal model and the measured data. In order to obtain the bolometer's effective responsivity, the conversion ratio of optical to electrical power must be known. This is obtained by normalizing the optical responsivity curves to the power dissipated in the bolometer [7]. Using Eq. (7), a graph of the temperature versus ESD-induced voltage for a step function ESD event can be obtained.

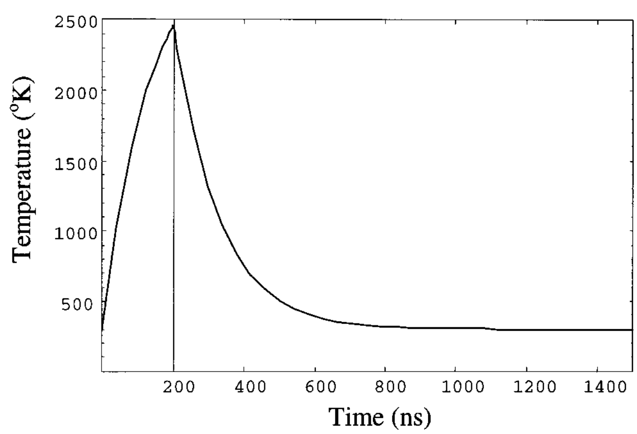

Figure 1 Temperature versus time graph obtained using the proposed thermal model for a 197 Ω microbolometer when a 200 ns, 1 V ESD square pulse is applied

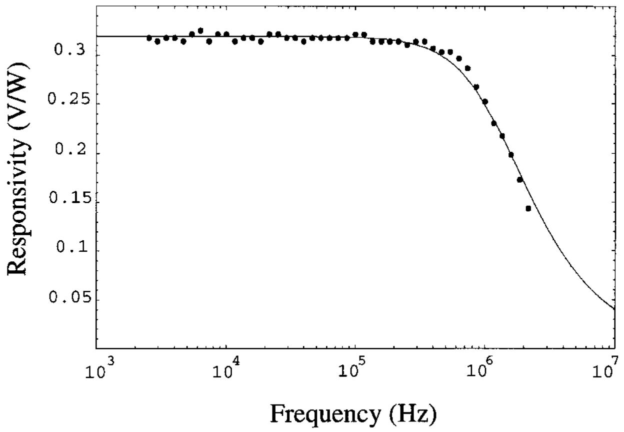

Figure 2 Responsivity measurements made on a 197 Ω niobium microbolometer, and fitted to the proposed thermal model with $R_{th} = 71 \times 10^5$ K/W and $C_{th} = 1.78 \times 10^{-14}$ J/K. This microbolometer had a time constant of 127 ns

This describes the steady-state thermal behavior of the microbolometer after a voltage is applied. Figure 3 illustrates this behavior for a 197 Ω niobium microbolometer, showing that the microbolometer's temperature reaches the melting point of niobium at a voltage of 0.68 V. Destructive tests were performed on eight microbolometers with resistances of 195 ± 5 Ω and time constants of 123 ± 6 ns. A failure voltage of 0.65 ± 0.05 V was recorded for these devices. The temperature versus voltage curve shown in Figure 3 is useful in determining the vulnerability of the microbolometer to the biasing voltage. It is also useful for the determination of the initial temperature conditions of the bolometer, that is, the initial temperature caused only by the ambient temperature and the bias voltage. The power-to-failure versus time-to-failure curve [10] is used to explain the relationship of physical failure to a critical temperature (melting temperature). Figure 4 shows a graph of this type for a 197 Ω Nb microbolometer. This graph was obtained using Eq. (7) and plotting power P_{ESD} versus the time t when the temperature reaches niobium's melting point (failure criteria). The parameters R_{th} and C_{th} necessary to generate the graph were obtained from data measured on the Nb microbolometer.

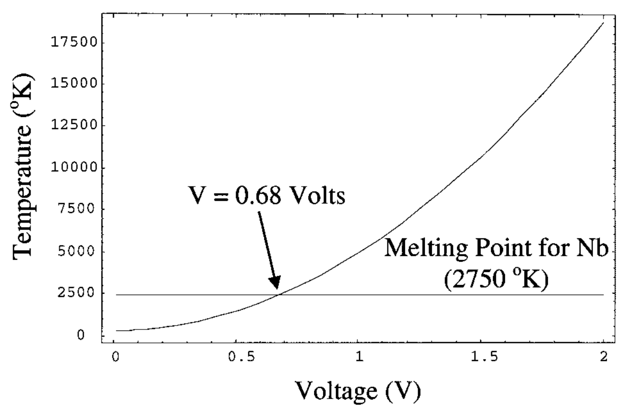

Figure 3 Temperature versus applied voltage on a microbolometer. This graph was obtained using the proposed thermal model for a 197 Ω microbolometer. The voltage needed to destroy the microbolometer (0.68 V) is within 5% of the value obtained by destructive tests performed over microbolometers in the laboratory

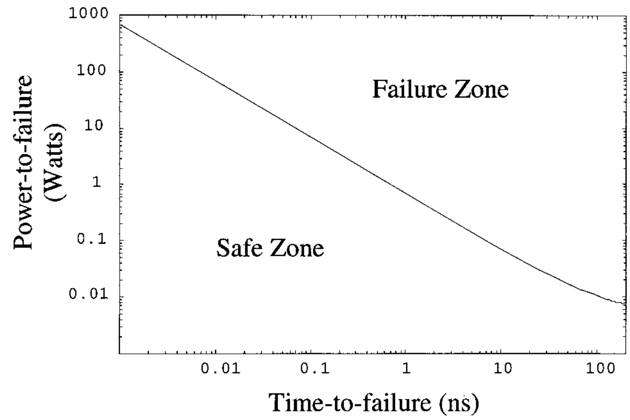

Figure 4 Power-to-failure versus time-to-failure graph obtained using the proposed thermal model for a 197 Ω microbolometer

The power-to-failure versus time-to-failure graph gives the power rating and the time response the protection circuit needs to have to effectively protect against ESD events.

IV. CONCLUSION

An empirical thermal model was used to characterize the response of microbolometers to electrical stress. This thermal model can be used to make a power-to-failure versus time-to-failure analysis, and therefore determine the robustness of the microbolometers and the protection needed to shield them from ESD events. This model can be used with any kind of microbolometer, and is independent of the geometry, fabrication process, and materials used. The unknown parameters R_{th} and C_{th} for the thermal model are fitted to data obtained by direct measurement of the temporal responsivity.

REFERENCES

1. S.E. Schwarz and B.T. Ulrich, Antenna-coupled infrared detectors, J Appl Phys 48 (1977), 1870–1873.
2. J. Alda, C. Fumeaux, M.A. Gritz, D. Spencer, and G.D. Boreman, Responsivity of infrared antenna-coupled microbolometers for air-side and substrate-side illumination, Infrared Phys Technol 41 (2000), 1–9.
3. C. Duvvury and A. Amerasekera, ESD: A pervasive reliability concern for IC technologies, Proc IEEE 81 (1993), 690–702.
4. J.S. Smith, General EOS/ESD equation, EOS/ESD Symp 97 Proc 1997, pp. 59–67.
5. N. Mohan, T.M. Undeland, and W.P. Robbins, Power electronics, converters, applications, and design, Wiley, New York, 2nd ed., 1995, pp. 733–737.
6. N. Khurana, T. Maloney, and W. Yeh, ESD on CHMOS devices —Equivalent circuits, physical models, and failure mechanisms, Proc IEEE Int Rel Phys Symp, 1985, pp. 212–223.
7. D.P. Neikirk, W.L. Wayne, and D.B. Rutledge, Far-infrared microbolometer detectors, Int J Infrared Millimeter Waves 5 (1984), 245–278.
8. I. Codreanu, C. Fumeaux, D.F. Spencer, and G.D. Boreman, Microstrip antenna-coupled infrared detector, Electron Lett 35 (1999), 2166–2167.
9. J. Alda, C. Fumeaux, I. Codreanu, J.A. Schaefer, and G.D. Boreman, Deconvolution method for two-dimensional spatial-response mapping of lithographic infrared antennas, Appl Opt 38 (1999), 3993–4000.
10. D.C. Wunsch and R.R. Bell, Determination of threshold failure levels of semiconductor diodes and transistors due to pulsed voltages, IEEE Trans Nucl Sci NS-15 (1968), 244–259.